CrossMark

ORIGINAL ARTICLE

The rat corticospinal system is functionally and anatomically segregated

Rafael Olivares-Moreno[1] · Yunuen Moreno-Lopez[1] · Luis Concha[2] ·
Guadalupe Martínez-Lorenzana[1] · Miguel Condés-Lara[1] · Matilde Cordero-Erausquin[3] ·
Gerardo Rojas-Piloni[1]

Abstract The descending corticospinal (CS) projection has been considered a key element for motor control, which results from direct and indirect modulation of spinal cord pre-motor interneurons in the intermediate gray matter of the spinal cord, which, in turn, influences motoneurons in the ventral horn. The CS tract (CST) is also involved in a selective and complex modulation of sensory information in the dorsal horn. However, little is known about the spinal network engaged by the CST and the organization of CS projections that may encode different cortical outputs to the spinal cord. This study addresses the issue of whether the CS system exerts parallel control on different spinal networks, which together participate in sensorimotor integration. Here, we show that in the adult rat, two different and partially intermingled CS neurons in the sensorimotor cortex activate, with different time latencies, distinct spinal cord neurons located in the dorsal horn and intermediate zone of the same segment. The fact that different populations of CS neurons project in a segregated manner suggests that CST is composed of subsystems controlling different spinal cord circuits that modulate motor outputs and sensory inputs in a coordinated manner.

Keywords Spinal cord · Sensorimotor cortex · Layer 5 pyramidal neurons · Dorsal horn · Corticospinal

Abbreviations
CST	Corticospinal tract
CS	Corticospinal
PAD	Primary afferent depolarization
EFPs	Evoked field potentials
SD	Standard deviation
M1	Primary motor cortex
S1	Primary somatosensory cortex
M2	Secondary motor cortex
S2	Secondary somatosensory cortex
HL	Hind limb
FL	Fore limb

Rafael Olivares-Moreno and Yunuen Moreno-Lopez are equally contributed.

✉ Gerardo Rojas-Piloni
piloni@unam.mx

1   Departamento de Neurobiología del Desarrollo y Neurofisiología, Instituto de Neurobiología, Universidad Nacional Autónoma de México, Campus UNAM-Juriquilla, Querétaro, Mexico

2   Departamento de Neurobiología Conductual y Cognitiva, Instituto de Neurobiología, Universidad Nacional Autónoma de México, Campus UNAM-Juriquilla, Querétaro, Mexico

3   Institut des Neurosciences Cellulaires et Intégratives, UPR 3212 CNRS, Strasbourg, France

Introduction

The corticospinal (CS) tract is a complex multifunctional system present in all mammals (Lemon and Griffiths 2005; Lemon 2008). The CS descending projection in different species plays a major role in voluntary motor control, which results from direct and indirect modulation of spinal cord pre-motor interneurons (Jankowska et al. 1976; Porter and Lemon 1993; Maier et al. 1998; Edgley et al. 2004; Maeda et al. 2016). This system is also involved in a selective and complex modulation of sensory information (Eguibar et al. 1994; Lomeli et al. 1998; Moreno-Lopez

 Springer

et al. 2013), which is important for the proper execution of volitive movements (Hultborn et al. 1987a, b; Seki et al. 2003; Fink et al. 2014).

In different species from rodents to primates, the role of the CS pathway in motor control, especially in the control of fine movement, is well established (Lawrence and Kuypers 1968; Porter and Lemon 1993; Maier et al. 1998; Nakajima et al. 2000; Lemon 2008). The motor execution driven by the CS projection could be due to direct modulation of ventral horn motoneurons which, in turn, drive muscle activity (Rathelot and Strick 2009; Griffin et al. 2015); or due to indirect modulation of the motoneuron activity mainly via pre-motor interneurons (Alstermark and Pettersson 2014; Bourane et al. 2015).

In addition, several areas of sensorimotor cortex exert primary afferent depolarization (PAD) in muscular and cutaneous afferent fibers (Carpenter et al. 1963; Andersen et al. 1964; Abdelmoumene et al. 1970; Rudomin et al. 1986; Rojas-Piloni et al. 2010; Moreno-Lopez et al. 2013). This CS modulation of primary sensory afferents is very selective (Eguibar et al. 1994; Lomeli et al. 1998), indicating that sensory information with a common source may be uncoupled, which is relevant for motor control and proper execution of movements (Nelson 1996). Moreover, sensory inputs are modulated during voluntary movement in non-human primates (Seki et al. 2003) as well as in humans (Hultborn et al. 1987a, b), and recently, it was demonstrated that the performance of skilled voluntary movements is determined by GABAergic interneurons responsible for segmental presynaptic inhibition (Fink et al. 2014).

CST originates from multiple motor and somatosensory cortices (Galea and Darian-Smith 1994; Ullan and Artieda 1981; Miller 1987; Lemon 2008) and their axons terminate in all gray matter of the spinal cord (Armand 1982); however, in rodents and marsupials, the influence of the CS projections on the spinal gray matter is exerted largely through interneurons in the sensory dorsal horn. However, the CS fiber terminations in the gray matter of carnivores are denser in ventral zones, contacting interneurons of the lamina VII. In primates, CS terminals reach motoneuron cell columns (lamina IX), indicating that CS terminations are closer to motor output, the higher the species is on a phylogenetic scale; for review, see (Schieber 2007; Welniarz et al. 2016). Hence, descriptions of the CS system in rodents are not necessarily applicable to the primates due to several crucial differences between species. Yet, the neuronal networks underlying direct interactions between sensory and motor functions in the spinal cord are beginning to be unraveled (Bourane et al. 2015), although little is known about the organization of CS projections, the intracortical microcircuitry, and the synaptic interactions in

the sensorimotor cortex that may encode different cortical outputs to the spinal cord.

The purpose of the present study was to evaluate if the CST is composed of segregated subsystems controlling different spinal cord circuits. The functional segregation of the CS system has long been suggested (for review, see Lemon and Griffiths 2005), but has never been conclusively shown. Here, we report that in the rat, different CS neurons activate with a different time latency, distinct dorsal horn, and intermediate zone neurons of the same segment of the spinal cord. This segregation supports the idea of a functional compartmentalization among layer 5 output corticospinal neurons.

Materials and methods

All procedures were carried out in accordance with the recommendations of the National Institutes of Health Guide for the Care and Use of Experimental Animals and were approved by the local Animal Research Committee of the Instituto de Neurobiología at Universidad Nacional Autónoma de México. Male Wistar rats were used for this study. All the animals were housed individually in a temperature-controlled (24 °C) colony room and maintained on a 12-h/12-h light/dark cycle (lights on at 7:00 a.m.). Food and water were provided ad libitum.

Electrophysiological recording and stimulation

For electrophysiological experiments, 57 rats were used. Rats (280–300 g) were anesthetized with urethane (1.4 g/kg, i.p.). A cannula was inserted into the trachea to provide artificial ventilation. End-tidal CO_2 concentration was continually measured by means of a capnograph monitor (Surgivet VT90041), and tidal air volume was adjusted to have a stable CO_2 concentration of 4.5%. The electrocardiogram was monitored during the experiment, and the core temperature was kept at 37 °C by means of a heating pad. During the experiment, the depth of the anesthesia was evaluated by tail and toe pinch reflexes. In case of reflex observed, an additional dose of 10% of the initial dose of urethane was administered to assure the acceptable depth of anesthesia. The rats were fixed in a stereotaxic apparatus (Narishige SR-6R) and secured in a spinal cord unit frame (Narishige STS-B), thus fixing vertebrae to improve stability at the recording site. A laminectomy was performed to expose spinal cord segments L3–L5 or C4–C6, and the surface of the exposed spinal cord was irrigated with saline solution.

Intraspinal cortical evoked field potentials (EFPs) were recorded with glass micropipettes filled with 1.2 M NaCl (tip diameter, 1.0–2.5 µm; 1.2–1.7 MΩ). EFPs were

recorded with the preamplifier filters set to a bandwidth of 0.3 Hz–10 kHz. During the experiment, all recordings were digitalized and stored for further processing. EFPs were recorded at different depths (100-μm intervals) in four parallel tracks separated by 500 μm. At each depth, averaged EFPs ($n = 16$ trials) produced by contralateral cortical stimulation were obtained. The stimulation electrodes were placed in the center of the sensorimotor cortex where the CS cells projecting to the lumbar (3 mm from the midline and −2.5 mm posterior to Bregma) or cervical (5 mm from the midline and −1 mm posterior to Bregma) spinal cord are located (Condes-Lara et al. 2007; Rojas-Piloni et al. 2010; Paxinos and Watson 1998). To avoid damage to the corticospinal cells, the stimulation electrodes were placed at the superficial border of the inner pyramidal cell layer (1000 μm below the cortical surface). Cortical stimulation consisted in trains of pulses (pulse duration 0.1 ms, inter stimulus interval 1 ms, 100–300 μA); a single cortical stimulus evokes negligible spinal cord responses, then the number of stimuli of the stimulation train was determined increasing the number of pulses until the intraspinal EFP reaches a maximal amplitude. Usually, trains of five pulses were used (Supplementary Fig. 1). To compare the EFPs recorded at different depths, the amplitudes of the EFPs in each experiment were measured at the same latency using as a reference the time in which we observed the maximal negativity of the EFP with maximal amplitude. In this way, at each recording depth, the amplitude of the averaged EFPs was measured with a fixed latency after the last cortical stimulus. Isopotential contours were plotted with amplitude values for each location using a linear interpolation on a set of X, Y, and Z triplets of the matrix. Then, the isopotential contours for the cortical EFPs were superimposed on the metric plane of the images of spinal cord atlas (Sengul 2013).

Single-unit extracellular recordings were recorded at lumbar L3–L5 segments by means of glass micropipettes filled with 1.2 M NaCl (5–10 MΩ), and the neuronal responses produced by contralateral cortical or neuronal receptive field (RF) electrical stimulation were analyzed. The extent of each neuron's RF was mapped by a series of manual stimulations applied with a Von Frey Filament (0.07 g). Then, the RF electrical stimulation was applied by means of two fine subdermal electrodes, connected to a stimulus isolator unit, inserted into the center of particular somatic RF for each recorded neuron. This stimulation consisted of single pulses of 1-ms duration at 0.5 Hz with intensities starting at 10 μA and increasing until a threshold was reached for each cell.

In addition, in 15 experiments, extracellular recordings from CS neurons projecting to lumbar segments were performed in the sensorimotor cortex with glass micropipettes filled with 1.2-M NaCl (5–10 MΩ). To identify the CS neurons, a concentric bipolar stimulating electrode (MicroProbes CEA 200) was placed in the contralateral CST (dorsal funiculus at L4 level). Antidromic spike responses, evoked by stimulation of the contralateral CST, were tested with single, 0.1-ms square pulse with intensities starting at 100 μA and increasing until a threshold was reached for each cell, but never exceeding 300 μA. When a stable cell recording was obtained, the following criteria were used to establish the antidromic characteristic of the cell responses: a constant threshold and latency, the ability to follow a stimulus train of 333 Hz and a collision of the orthodromic spikes with antidromic evoked spikes. We used the spontaneous action potentials of sensorimotor cortex recorded neurons to trigger the electrical stimulation CST with a variable delay. Systematically changing the delay between the spontaneous spikes and CST stimulation allowed us to measure the critical period in which collision between spontaneous and evoked action potentials occurs. Neurons that did not satisfy these criteria were excluded, because they were activated by synaptic interactions.

Fluorescent labeling of CS neurons

To analyze the distribution of CS neurons projecting to different areas of the same spinal cord segment, neuronal tracers were used. Hence, adult (P50–P55, $n = 6$) rats of both sexes were anesthetized with a ketamine/xylazine mixture (70/6 mg/kg, i.p.) and fixed on a stereotaxic frame (Kopf Instruments 900LS). A laminectomy was performed, followed by an incision of the dura to expose cervical (C4–C5) or lumbar L3–L4 spinal cord segments. Cholera toxin subunit b recombinant conjugated with Alexa 488 and 594 (Molecular Probes; 1 mg/mL in PBS) were injected into the dorsal horn and intermediate zone of same segment (cholera toxin-488 in the dorsal horn and -594 for the intermediate zone) of the spinal cord. For the cervical segments, the dorsal horn injections were made 850 μm lateral to the midline, and the tip of the pipette was set at a depth of 400 μm. The cervical intermediate zone injections were made 700 μm lateral to the midline, and the tip of the pipette was set at 1300-μm depth. Lumbar segments injections were made 700 μm lateral to the midline for the dorsal horn and at 300 μm depth. The lumbar intermediate zone injections were made 600 μm lateral to the midline, and the tip of the pipette was set at 1100 μm depth. To perform discrete tracer injections, graduated glass micropipettes (BLAUBRAND® intraMARK) with a tip diameter between 10 and 25 μm were coupled to a pneumatic picopump (PV830, WPI). Before each injection, tip diameter of the micropipette was measured, and the pressure and pulse duration were calibrated to adjust the amount injected. Usually, discrete injections (30–50 nL) were obtained using pressure pulses of 200 ms at 20 PSI.

After each injection, the pipette tip was kept for 3 min before removal. The wound was then closed with absorbable sutures.

Five days after the injections, the animals were deeply anesthetized (pentobarbital 45 mg/kg i.p.) and perfused through the heart with phosphate buffer 0.1 M, followed by paraformaldehyde (4% in 0.1-M phosphate buffer, pH 7.4). The brains and spinal cord were removed and stored overnight in vials containing the same fixative.

Image acquisition and analysis

Parasagittal brains and the tangential spinal cord sections were cut in a vibratome (Leica VT1200S) at 50-µm intervals. Only the experiments in which the injections were completely separated and located in the dorsal horn and intermediate zone of the same spinal segment were analyzed (Supplementary Fig. 2). The size of the injection sites was estimated automatically using the ImageJ software (V 1.50i) measuring the periphery of the zone stained with the tracer in the center of each injection and computing the transversal area. In this way, we only analyzed the experiments in which the size of the injections in the dorsal horn and intermediate zone was equivalent. Mosaic images (resolution 1.023 µm/pixel) of the sections containing the fluorescent retrograde-labeled cells were obtained in a fluorescence microscope (Zeiss AXIO Imager.Z1) attached to a digital camera (AxioCam MRm, 1.3 MP) using the appropriate filters (GFP for Alexa 488 and Rhodamine for Alexa 594) and acquired with a 10× objective (ZEISS Plan-APOCHROMAT, NA 0.45). Additional detailed images (resolution 0.66 µm/pixel) were acquired with a confocal microscope (Zeiss 780 LSM) using an objective LD PCI Plan-Apochromat 25×/0.8 Imm Korr DIC M27.

To better visualize the spatial distribution of the labeled neurons, the mosaic images were superimposed with the magnetic resonance imaging (MRI) atlas of the rat brain (Papp et al. 2014). This T2*-weighted atlas has isometric resolution of 39 µm, which allowed the visualization of parasagittal slices similar to the mosaics (Supplementary video 1). The histological mosaics were manually aligned with the MRI volume by selecting shared and clearly visible anatomical landmarks and using a linear transformation, as implemented in Amira version 5.6 (FEI, Hillsboro, OR, USA). Once the mosaic images were aligned with the atlas, the positions of the CS neuronal somas were labeled (Supplementary video 1). In this way, a 3D map of the CS neurons was obtained (Supplementary video 2). To compute relative neuron density, the soma distributions were obtained in 250 × 250-µm steps for the tangential plane, and vertical density profiles were computed in 50-µm steps along the vertical axes.

Fig. 1 Different populations of spinal cord neurons are activated by ▶ the CST. **a** Experimental design. The RF stimulation electrodes were located ipsilaterally to spinal cord recording, whereas cortical stimulation electrode was located contralateral to spinal recording. **b** Intraspinal EFP evoked by contralateral sensorimotor cortex stimulation showing early and late components. **c** Example of unitary extracellular electrophysiological response (*red trace*) of a spinal cord neuron produced by sensorimotor cortex stimulation and peristimulus time histogram computed for 16 consecutive spiking responses. **d** Same as **c** but for another neuron with a longer latency response. Notice that short and long-latency spiking responses can be associated with the early and late components of the EFP, respectively. **e** Averaged peristimulus time histogram produced by cortical stimulation computed for 18 neurons with short (*black bars*) and 10 long (*gray bars*) latency responses. *Red and green lines* are the Gaussian fits for both histograms. The *upper bars* show the time distribution of the evoked action potentials of the neurons with short (*red*) and long (*green*) latency responses (*$p < 0.0001$, Mann–Whitney U). **f, g** Example of spiking responses evoked by electric stimulation of the receptive field (RF) (represented in the *inset paw drawing*) and peristimulus time histograms of the same neurons recorded in **c** and **d**. **h** Averaged peristimulus time histogram produced by RF stimulation computed for the same neurons in **e**. **i** Relationship between mean activation latency ($n = 16$ consecutive responses) of the first evoked action potential, produced by cortical stimulation, and the SD of this latencies for 28 recorded neurons. Clustering analysis reveals two populations of neurons with different latencies; covariance matrices are represented as confidence ellipsoids. *Asterisks* in data points indicate the neurons illustrated in **c** and **d**

Statistics

All the recorded EFPs were averaged (16–24 sweeps) and analyzed off line with the Clamfit software (pCLAMP 10.0, Molecular Devices). Statistical analyses were computed using nonparametric tests. The amplitudes of the control EFPs were compared using a Wilcoxon test. For multiple comparisons, a Kruskall–Wallis ANOVA and Friedman test were performed. The distribution of action potentials of spinal cord neurons, which occurred following cortical stimulation, was compared by means of a clustering analysis using a gaussian mixture model. The fraction (CS cells projecting to dorsal or intermediate zones divided by the total number of CS labeled cells) was compared with the Mann–Whitney U test. Differences were considered significant starting at $p = 0.05$.

Results

Spinal neurons driven by CS projection

To characterize the segmental neurons that are modulated by CS projections, single-unit recordings were performed in the lumbar dorsal horn (L3–L4). Twenty-eight neurons responding to cortical stimulation were recorded in 22 experiments. The delay, number, and frequency of spikes
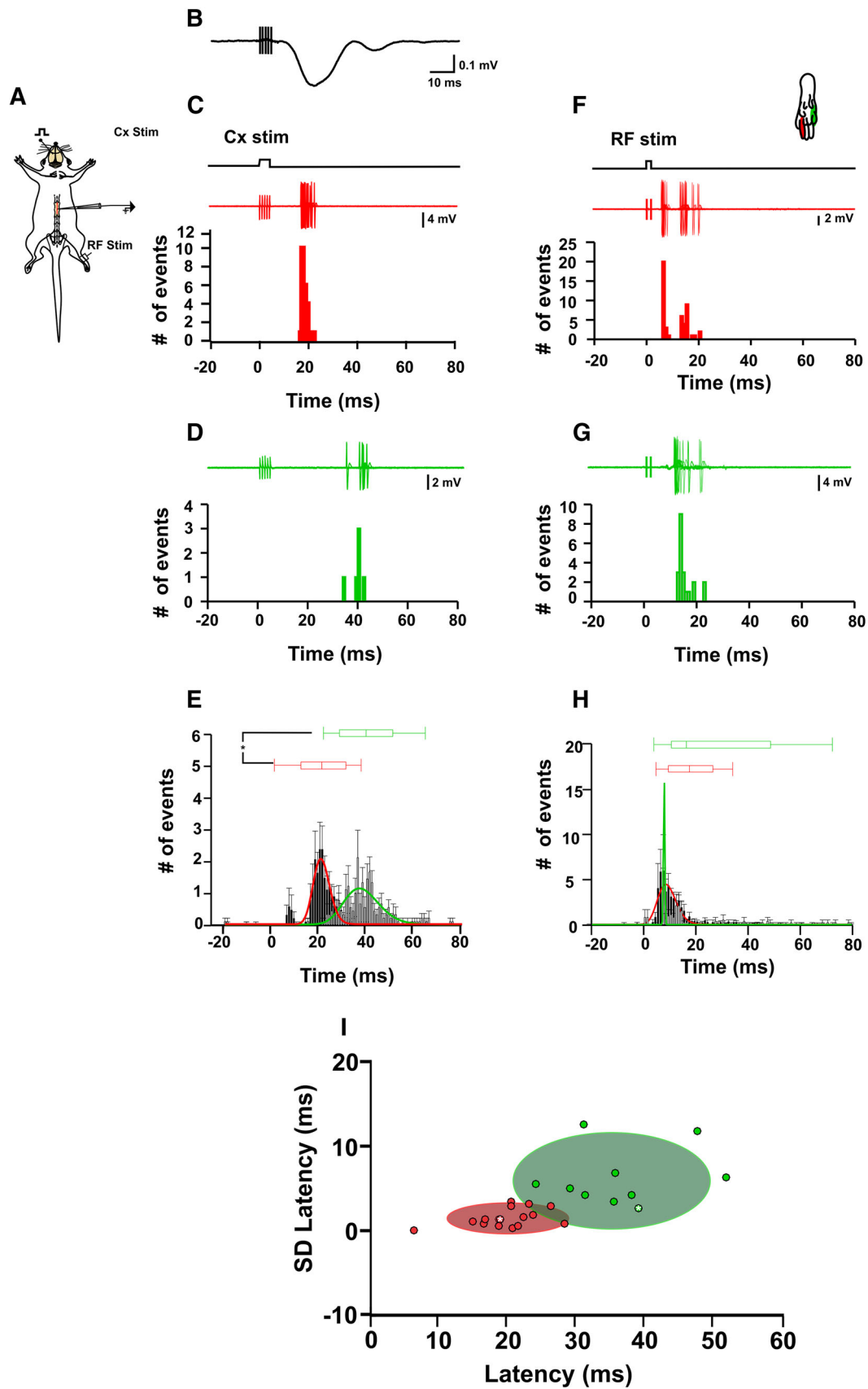
were highly variable from neuron to neuron. To draw out different response profiles, we analyzed the distribution of spike times after cortical stimulation (times of all the spikes evoked by cortical stimulation) from the 28 neurons altogether during the 80 ms following the last stimulus of cortical stimulation. This distribution was clearly not normal (Shapiro–Wilk normality test, $W = 0.91654$, $p < 2.2e-16$). It was best fitted by a sum of two gaussian functions (Fig. 1e), using R package 'mixtools' (Benaglia et al. 2009). This analysis suggests two response profiles: a first population highly synchronized, with a standard deviation (SD) of the spike times after cortical stimulation of 3.6 ms; the second is poorly synchronized, with an SD of the spike times after cortical stimulation of 14.7 ms. Furthermore, clustering analysis using a gaussian mixture model taking into account the activation latency of the first evoked action potential after last cortical stimulus and the SD of this latencies, we classified two classes of neurons (Fig. 1i): those with a short activation latency (average latency from the last stimuli to the first evoked action potential 19.0 ± 0.3 ms; recording depth 282.1 ± 37.6 μm; $n = 18$) and those with long activation latency (average latency 34.5 ± 0.7 ms; recording depth 353 ± 40.3 μm; $n = 10$). The latencies of the responses were statistically different in the two groups ($p < 0.0001$, Mann–Whitney U test). Interestingly, both types of neurons showed cutaneous RF (Fig. 1f–h). The RF were small and, when activated by electric stimulation, had low activation thresholds (10–100 μA). The latency of activation after cutaneous electrical stimulation (28.9 ± 2.4 ms) indicates that these neurons also receive information from Aβ fibers (Fig. 1h). No differences were observed in the mean number of action potentials evoked to RF stimulation between both (short and long activation latency after cortical stimulation) classes of neurons. These results indicate that in the spinal cord neurons, there is synaptic convergence of CS projections and low-threshold sensory primary afferents.

To analyze the distribution of spinal cord cells responding to cortical stimulation within the spinal cord, the spinal EFP was analyzed. In both cervical and lumbar enlargements, the intraspinal cortically evoked EFP showed two components with different latencies. For the cervical segments, the short-latency response had a maximal negativity at 11.2 ± 0.8 ms and the long-latency response at 38.5 ± 0.1 ms ($n = 6$) after cortical stimulation. For EFP recorded at lumbar segments, the latencies were 21.9 ± 0.1 and 48.3 ± 0.3 ms ($n = 7$). The cervical EFP was more complex than lumbar, and commonly, the short-latency component exhibited two bumps. To analyze the intraspinal location of the interneurons activated by cortical stimulation, the EFP was recorded at different depths, every 100 μm, in four parallel tracts. As can be
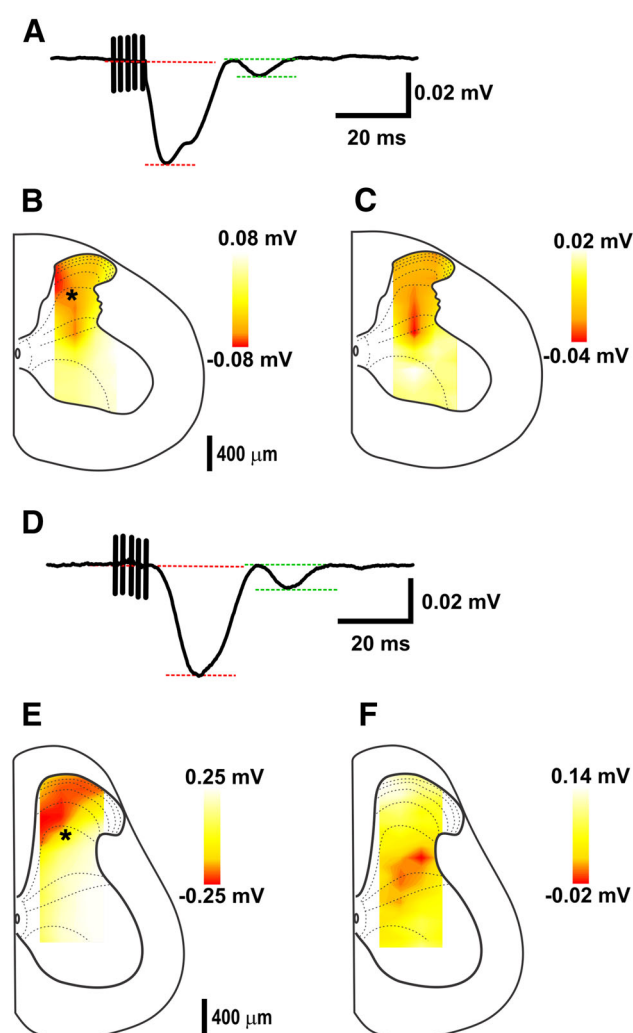

Fig. 2 Map of intraspinal EFP driven by CST stimulation. a Averaged EFP produced by cortical stimulation recorded in cervical segment C4. The *dashed lines* represent the magnitude of the short- (*red*) and long- (*green*) latency components. b Drawing of the cervical segment C4 superimposed with the mean isopotential contours for the intraspinal EFP short-latency responses produced by cortical stimulation. The amplitude of the short-latency responses was measured as indicated by the *red dashed lines* in **a**. c The same as **b** but for the EFP long-latency responses produced by cortical stimulation (measured as indicated by *green dashed lines* in a). The isopotential *contours* are superposed on the metric plane of the spinal cord outline drawn from the histological images obtained from the spinal cord atlas (Sengul 2013). *Asterisk* in the drawings bellow represents the zone in which the illustrated recordings were performed **d–f**, same as **a–c** but for the lumbar EFPs

observed in Fig. 2, each EFP component (short and long latency) had its maximum amplitude in very different loci within the gray matter. Hence, in both cervical and lumbar segments, maximal negativity of the short-latency component of the EFP was located more superficially (laminae II–IV) than the one of the long-latency component (deep lamina V–VII) (Fig. 2). Moreover, the intraspinal depths in which the short-latency components show a maximal

amplitude (525 ± 160 μm for lumbar and 450 ± 189 μm for cervical) are significantly more superficial than the depths which long-latency components (1225 ± 149 μm for lumbar and 900 ± 129 μm for cervical) are largest ($p < 0.05$, Student t test).

In three experiments, we investigated if a direct CS connection produces both components of the intraspinal EFP (Fig. 3). Indeed, both components of intraspinal EFP evoked by cortical stimulation were reduced significantly after pyramidal tract electrolytic lesions (DC current 10 μA, 10 s): the long-latency peak was reduced 75.4 ± 9.7%, and the short-latency peak 57.6 ± 7.5% with respect to control ($p = 0.0002$ and $p = 0.0004$,

respectively, Mann–Whitney U test). None of our experiments revealed a complete lesion of the pyramids, the degree of the lesion was 62.5 ± 3.9% ($n = 3$). However, the latency of the remaining EFPs after lesion did not change and we never observed a reduction in the amplitude of the EFPs when the lesion was produced outside the pyramidal tract, indicating that an intact CST is necessary for both the short- and long-latency spinal EFP.

We investigated if short- and long-latency neuronal spinal cord responses evoked by cortical stimulation are produced by the activation of CS cells with different conduction velocity. Then, we performed single-unit recording of CS neurons in S1 hind-limb area as well as in M1, and evoked antidromic spikes by stimulating the lumbar spinal dorsal funiculus (Fig. 4a, b). In this way, the measured conduction times computed for 28 CS neurons recorded in 15 experiments was not unimodal (Hartigans' dip test, $D = 0.078571$, $p = 0.1688$). Moreover, using a gaussian mixture model, the distribution of the conduction time, and recording depths, it was best fitted by a sum of two Gaussian functions with conduction time averages in 17.1 and 35.8 ms (Fig. 4e). The estimated conduction velocities ranged from 2 to 8 m/s (distance 9.5 cm). These velocities are in the same range as the ones calculated for the spinal EFP evoked by cortical stimulation: for the cervical EFP, the calculated conduction velocity for the short and long-latency EFP is, respectively, 6.5 ± 0.2 and 1.2 ± 0.01 m/s ($n = 6$), and similarly, for the lumbar EFP, they are, respectively, 5.1 ± 0.06 and 2.2 ± 0.06 m/s ($n = 7$). This result suggests that the short- and long-latency neuronal responses recorded in the spinal cord could be due to activation of CS neurons with different conduction velocities and located at different depths bellow cortical surface. Thus, to know if different populations of neurons project to different zones of the same segment of the spinal cord, retrograde neuronal tracing experiments were performed.

Distribution of CS neurons projecting to dorsal and intermediate zone

Electrophysiological results suggest that different populations of CS neurons project to dorso-ventral positions within the spinal cord. To confirm this idea, we injected into the same spinal cord segment of two different neuronal tracers: cholera toxin conjugated with Alexa 488 and 594 (Conte et al. 2009), respectively, injected in the intermediate zone and dorsal horn. Five days after injection, the animals were perfused for histological processing of the brain and spinal cord. The distribution of CS cells was analyzed only in the experiments (3 for lumbar and 3 for cervical segments) in which both injection sites were located in the same spinal cord segment, and the spread of the tracers was completely separated, including the gray
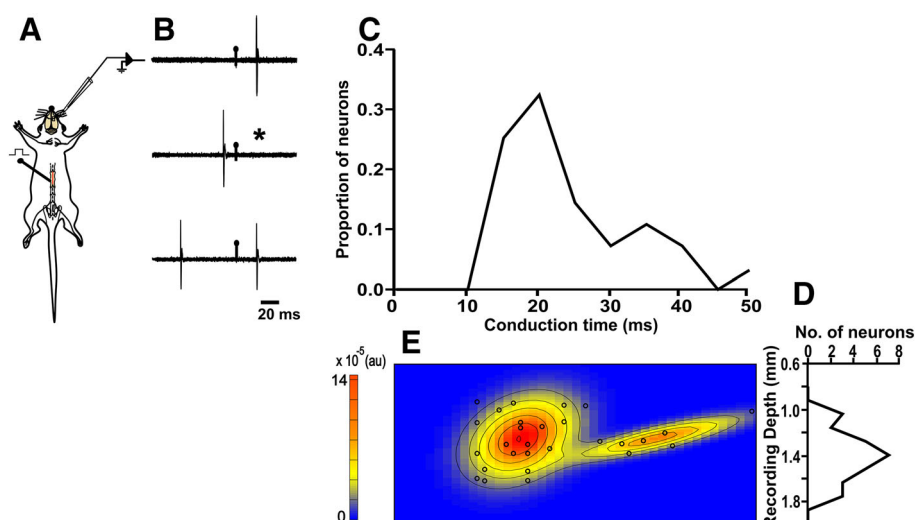

Fig. 3 Intraspinal EFPs evoked by cortical stimulation are suppressed after pyramidal tract lesions. **a** Averaged intraspinal EFPs evoked by contralateral cortical stimulation recorded simultaneously in cervical (C5) (*left trace*) and lumbar (L4) (*right trace*) segments before electrolytic lesion of the ipsilateral pyramidal tract at the medullary level. **b** Same as **a** but after pyramidal tract lesion in the same experiment. **c** Schematic drawings showing the extension of the electrolytic lesions in three different experiments. **d** Absolute amplitudes of the short-latency intraspinal EFP (indicated by the *red arrows*) before and after the lesion produced in the pyramidal tract (the *bars* represent mean ± SE). **e** The same as **c** but for long-latency component EFP (green arrows). *Asterisk* $p < 0.005$, Mann–Whitney U

Fig. 4 Antidromic identification of CS neurons. **a** Experimental setup. **b** Representative electrophysiological antidromic responses evoked by contralateral dorsal funiculus stimulation at lumbar level L4. The traces occurred in a sequential manner. The first trace shows five superimposed recordings of a corticospinal cell in which the evoked action potential appears with a fixed latency (19 ms) after the stimulus artifact (represented by the *vertical line* and *circle*). The second trace shows the collision test when the preceding orthodromic action potential occurs below the antidromic latency (see "Materials and methods"). The *asterisks* indicate the point at which the antidromic response would have occurred. The third trace shows that when the orthodromic action potential occurs above the antidromic latency, the collision of antidromic response does not occur. **c** Frequency distribution of the conduction times of all ($n = 28$) the CS cells recorded. **d** Distribution of recording depths of CS identified cells. **e** Gaussian mixture distribution fitting. The scale of X (conduction time) and Y (recording depth) axes corresponds to the scale of **c** and **d**. Individual data for all recorded neurons are indicated in *circles*

matter dorsal horn (laminae I–V) and the intermediate zone (Laminae VII). In addition, to obtain a 3D representation of the CS neuron density, the histological mosaic images were aligned with the MRI images (Fig. 5d; Supplementary videos 1 and 2).

In rodents, the CS neurons are widely distributed in the cerebral cortex (Ullan and Artieda 1981; Kamiyama et al. 2015) in the areas corresponding to the primary sensory cortex (S1), primary motor cortex (M1), the rostral part of secondary motor cortex (M2), and the secondary sensory cortex (S2). Here, we found that the relative contribution of cortical territories in which CS neurons are located is as follows: M1 $26.9 \pm 3.6\%$, S1 $49.5 \pm 6.7\%$, M2 $4.6 \pm 2.1\%$, and S2 $18.8 \pm 9.7\%$. However, the CS neurons projecting to the intermediate zone tend to be localized in rostral areas, and those projecting to the dorsal horn are found in the caudal part of the cortex, including S2. Moreover, in the sensorimotor cortex (areas S1FL and M1), the two cell populations are intermingled (Fig. 6a). Something similar was observed in the CS cells projecting to the lumbar enlargement (L3–L4); nevertheless, the distribution of the cells was restricted mainly to the areas corresponding to medial part of M1 and hind limb S1 (Fig. 6b). No CS neurons projecting to lumbar segments were located in S2.

All the CS cells projecting to the dorsal horn and intermediate zone were located intermingled in layer 5.

However, in M1 and S1, cells projecting to cervical intermediate zone were located deeper than CS neurons projecting to dorsal horn (Fig. 7). No differences were observed among S1 CS neurons projecting to lumbar segments, or among S2 or M2 CS neurons (Mann–Whitney U). In addition, the soma size of the cells projecting to the dorsal horn (17.4 ± 2.4 μm) and the cells projecting to deeper laminae (17.1 ± 2.1 μm) is not statistically different. Soma size of the pyramidal CS neurons reported herein is in the same range as the size reported previously for the subcortical projection neurons of the rat somatosensory cortex (Killackey et al. 1989).

Although the injection site areas of the dorsal horn ($0.14 \pm 8.8 \times 10^{-3}$ mm^2; $n = 3$) and intermediate zone (0.14 ± 0.012 mm^2; $n = 3$) at cervical segments and the areas of the dorsal horn ($0.11 \pm 7.2 \times 10^{-3}$ mm^2; $n = 3$) and intermediate zone ($0.14 \pm 3.9 \times 10^{-3}$ mm^2; $n = 3$) at lumbar segments show a similar size ($p > 0.5$, Mann–Whitney U) (Supplementary Fig. 2), the total number of S1 CS neurons projecting to the cervical dorsal horn was larger than the number of S1 CS cells projecting to cervical intermediate zone (Table 1). Furthermore, in M1, there are more neurons projecting to intermediate zone than to the dorsal horn in both cervical and lumbar segments. The same was observed in M2; however, no CS cells projecting to lumbar segments were observed in M2. In line with the electrophysiological results, the number of double-labeled
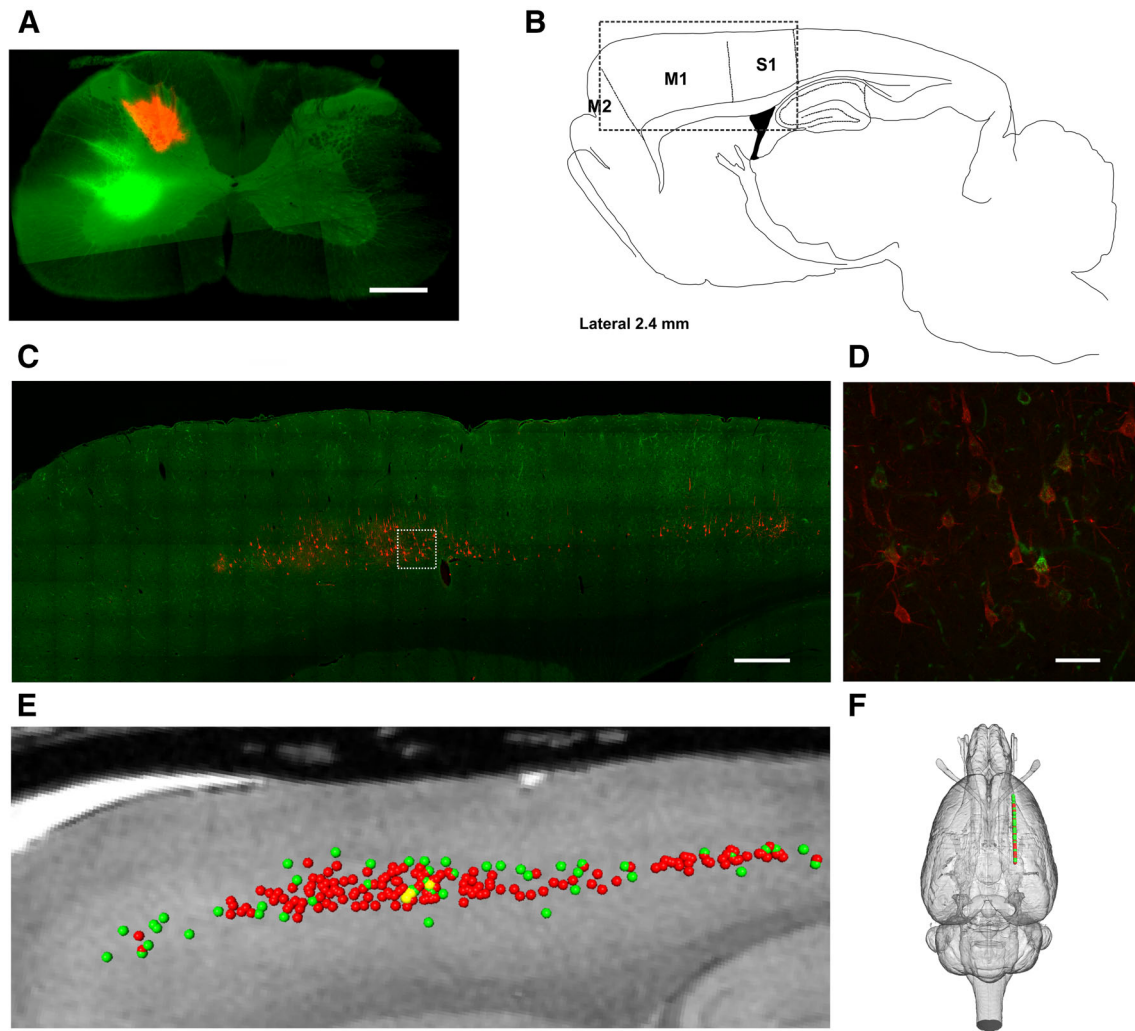
Fig. 5 Identification of retrogradely labeled CS cells projecting to the cervical dorsal horn and intermediate zone. **a** Photomicrography of the injection sites of the retrograde tracers (cholera toxin subunit B conjugated with Alexa 488 in *green* and Alexa 594 in *red*) into the contralateral dorsal horn and intermediate zone of cervical segment C4 in one experiment. **b** Schematic representation of a sagittal brain slice showing the location of the cortical areas that are the origin of the corticospinal tract (S2 not shown). **c** Mosaic photomicrograph of a single 50 μm parasagittal section of the sensorimotor cortex from the same experiment. The photomicrography was taken from the area indicated by the *dashed square* in **b**. **d** Detailed image of the area indicated in *dashed square* in **c**, showing some cells projecting to the superficial laminae of the contralateral dorsal horn (*red*) and intermediate zone (*green*). **e** Parasagittal view of the MRI atlas (Papp et al. 2014), onto which the labeled cells identified in the histological slices (**c**) were superimposed. **f** 3D representation of the rat brain showing the landmarks with the location of the same corticospinal labeled neurons in the *horizontal plane*. *Scale bars* 500 μm in **a**, **c** and 50 μm in **d**

cells was only $3.9 \pm 1.1\%$ for cervical and $2.1 \pm 1.4\%$ for lumbar segments (Table 1), indicating that segregated populations of CS neurons project to different gray matter laminae of the same spinal cord segment.

Discussion

Here, we show functional and anatomical evidence supporting the diversity of the CST. The results obtained, using the neuronal tracers and the bimodal distribution of antidromic conduction time observed in CS neurons, strongly suggest that at least two groups of CS neurons project in a segregated manner to the same segment of the spinal cord: one group projects to the dorsal horn, while the other projects to the intermediate zone. Moreover, the two groups of CS cells activate, with a distinct time latency, a different population of segmental neurons located in the dorsal horn, and intermediate gray matter, indicating that the CST is composed of subsystems controlling different spinal cord circuits that could modulate motor outputs and sensory inputs in a coordinated manner.

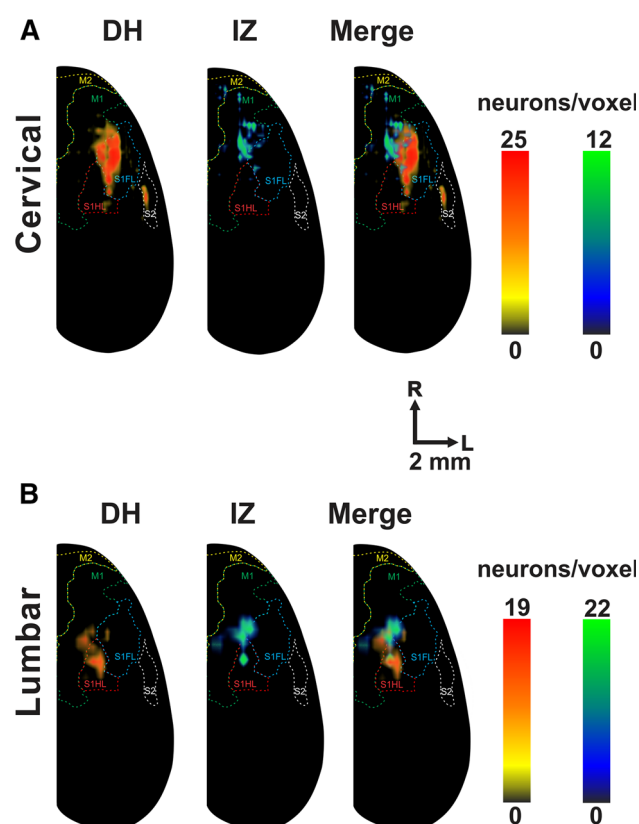Despite the use of very small injections of retrograde tracers, and in agreement with the previous observations

Fig. 6 Distribution maps of CS neurons projecting to dorsal horn and intermediate zone. **a** Averaged relative density representation maps ($n = 3$ animals) in the *horizontal plane* of the CS neurons projecting to the cervical (C4–C5), dorsal horn (DH *red*), and intermediate zone (IZ *green*). Neuron density is expressed as the mean number of retrograde-labeled neurons neurons/voxel ($250 \ \mu m^3$). The *merged maps* show the location of the cortical areas of M2, M1, S1FL (primary somatosensory fore limb), S1HL (primary somatosensory hind limb), and S2 cortices. Notice that there are three clusters of cells: a cluster located in M2 with cells projecting mainly to the intermediate zone; a second cluster in M1–S1 with both types of cells, which appear intermingled; a cluster in S2 with only CS cells projecting to the dorsal horn. **b** Same as **a** ($n = 3$ animals) but for CS neurons projecting to lumbar (L4) segment

(Ullan and Artieda 1981), we show an extensive distribution of CS neurons in different areas. The CS cells projecting to lumbar segments were distributed principally in S1HL and M1 of the sensorimotor cortex. However, CS neurons projecting to the cervical enlargement show a more complex distribution and were located in M1, M2, S1FL, and S2 (Fig. 6). Although there are some differences between species (Armand 1982), CST axons in rodents terminate in all gray matter of the spinal cord (Casale et al. 1988). Interestingly, between segments C3–C7, the CS projections are denser (Akintunde and Buxton 1992), and at C4–C5, the motoneurons innervating the majority of the muscles of the proximal and distal fore limb important for fine movements are located (Tosolini and Morris 2012). Moreover, microstimulation of those segments evoke

highly functional movements of the rat fore limb (Sunshine et al. 2013), indicating an overlap between corticospinal inputs and motor outputs to the fore limb. In agreement with the results reported here, in the upper cervical cord, the projections of primary and secondary somatosensory cortices ramify extensively in the most dorsal and lateral regions of the spinal cord, while the motor cortices project more ventrally (Suter and Shepherd 2015). We only analyzed the experiment in which injection sites were completely separated (Supplementary Fig. 2); however, some overlap could happen, even though it is not evident. In fact, when the injection of the tracers showed evident overlapping, we observed a large proportion of cells with both tracers (data not shown), indicating that the existence of double-labeled cells is due to some overlap of the tracers in the injection sites. In addition, it is shown that there is a clear segregation of some CS neurons after closely placed spinal injections. Nevertheless, as has been reported for the cortical neurons projecting to the dorsal column nuclei, which are closely located but segregated in cortex (Martinez-Lorenzana et al. 2001), we cannot discard that some of the segregation found in CS neurons might also be due to the uneven location of somatotopical representations along the rostrocaudal and dorso-ventral dimensions of the cord.

Early and late components of corticospinal neuronal responses

The conduction times measured in the anterograde spiking responses of the first evoked action potential after last cortical stimulus were 19.0 ± 0.3 ms for short-latency cells, and those with long activation latency were 34.5 ± 0.7 ms. These latencies are slightly higher than the retrograde conduction times. Differences could be explained, because the anterograde latency is the sum of the conduction time and the synaptic delays (1–2 ms), yet antidromic responses lack synaptic interactions, therefore, yielding retrograde conduction times always shorter than the anterograde latencies.

Although the soma size between the CS neurons projecting to different laminae of the spinal cord is very similar, the difference in the latency for the CST to activate superficial and deeper spinal cord neurons could be explained by the conduction velocities of CS neurons. Comparing the distributions of the activation latencies of the spinal cord neurons responding to cortical stimulation (Fig. 1e) and conduction times of CS cells (Fig. 4c, e), it is possible to assume that populations with different conduction velocities produce short- and long-latency intraspinal responses. In this way, based on the delay between cortical stimulation and intraspinal EFP, and assuming a direct connection, the early EFP component of the dorsal horn suggests the involvement of CS neurons

Fig. 7 CS neurons projecting to different spinal cord areas are intermingled in layer 5b of sensorimotor cortex. **a** Coronal sections showing CS cells of M1 projecting to the cervical dorsal horn (*red*) and intermediate zone (*green*). **b** Average density profiles (computed in 3 consecutive slices for 3 experiments) along the *vertical axes* of CS neurons projecting to the cervical (C4) dorsal horn (*red*) and intermediate zone (*green*) in M1. The histograms on the right show the fraction of CS cells projecting to the dorsal horn and intermediate zone in layer 5. **c** Same as **b**, but the distribution was computed for M1 projecting to lumbar segments. **d–f** Same as **a–c** but in S1. * $p < 0.05$, Mann–Whitney U. Scale bars 100 μm
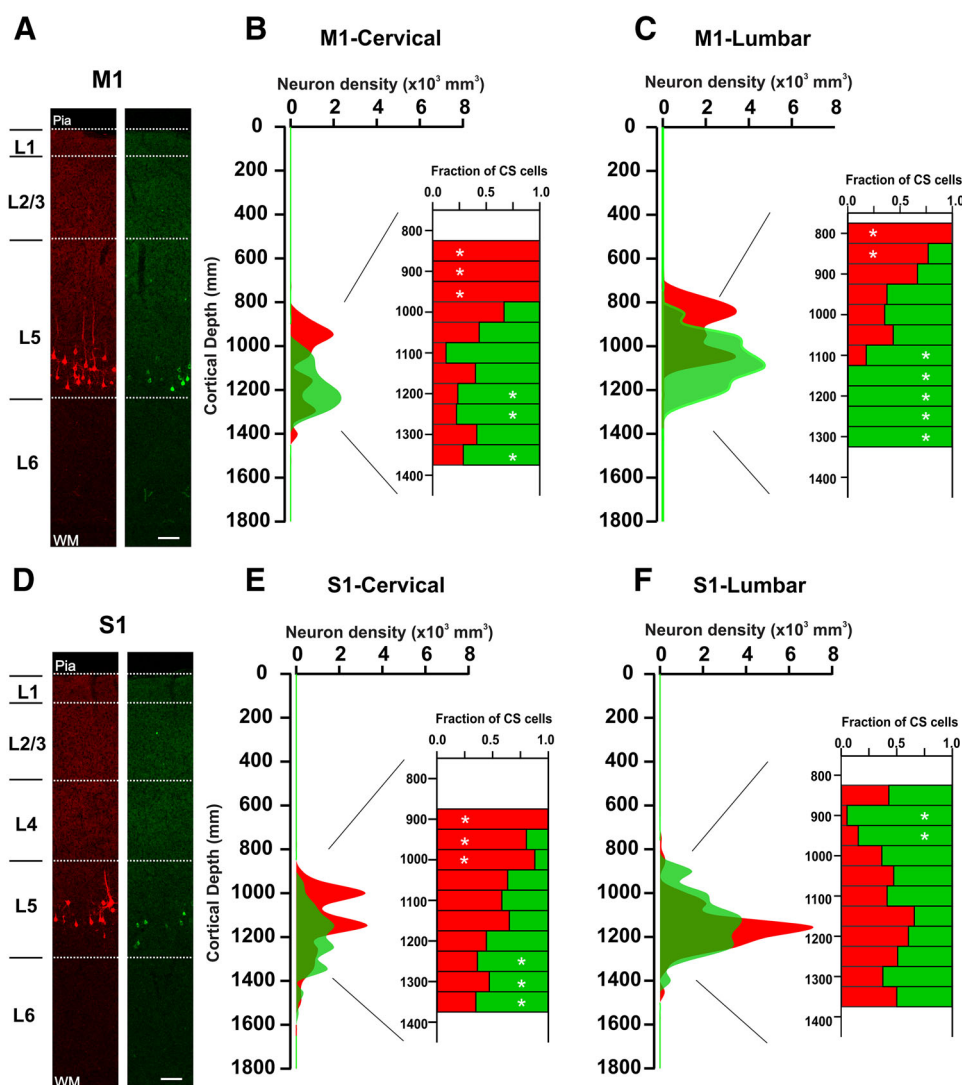
Table 1 Relative number of neurons projecting to dorsal horn (DH) and intermediate zone (IZ) in primary (S1) and secondary (S2) somatosensory, as well as primary (M1) and secondary (M2) motor cortices

%	M1	M2	S1	S2
Cervical (n = 3)				
DH	34.9 ± 13.5	29.1 ± 24.7	75.9 ± 13.2	100 ± 0.0
IZ	62.1 ± 13.2	70.9 ± 24.7	21.4 ± 11.5	–
Double	2.9 ± 1.4	–	2.5 ± 1.8	–
Lumbar (n = 3)				
DH	40.2 ± 3.6	–	44.3 ± 9.7	–
IZ	54.9 ± 3.2	–	53.6 ± 10.2	–
Double	4.8 ± 2.0	–	2.1 ± 1.4	–

Data are expressed as mean ± SE computed in six experiments (3 for cervical and 3 for lumbar injections)

Relative number of CS neurons projecting to the spinal cord

conducting at 1.2 ± 0.01 m/s for the cervical cord, and at 2.2 ± 0.06 m/s for the lumbar cord (mean 1.7 m/s) (distance between stimulation and recording electrodes cervical 4.5–5.5 cm; lumbar 9.5–10.5 cm). Similarly, the late component of the EFP recorded in deeper laminae suggests the involvement of CS neurons conducting at 6.5 ± 0.2 m/s for the cervical cord, and at 5.1 ± 0.06 m/s for the lumbar cord (mean 5.8 m/s). When directly measured, the conduction velocity of CS neurons varied between 2 and 8 m/s, suggesting that, indeed, both the short- and the long-latency EFP response could be due to a direct, CS innervation. The fastest descending fibers reported in the rat conduct at around 20 m/s (mean 9–13 m/s) (Mediratta and Nicoll 1983; Stewart et al. 1990; Babalian et al. 1993; Baker et al. 2001). However, estimates based on the fiber diameter of rat pyramidal neurons (0.5–1 μm) (Dunkerley and Duncan 1969; Leenen et al. 1985; Joosten and Gribnau

1988) result on lower conduction velocities, in the range of 2.4–6 m/s (Towe and Harding 1970), which agrees with the estimates reported here. The conduction times of the anti-dromic action potentials recorded in CS neurons show a clear bimodal distribution (Fig. 4c–e). In the sample of CS neurons recorded here, the minority of the cells show a slow conduction velocity. Nevertheless, it is possible that the neurons with higher conduction times, projecting to deeper laminae of the spinal cord and which are generally in the minority, could be missing from this sample.

Both short- and long-latency intraspinal responses significantly decreased after CST lesion (Fig. 3), indicating definitely that both travel by direct CST. However, EFPs were not entirely abolished, which could be due to the incomplete lesion of the pyramids or to the participation of other descending pathways like the reticulospinal or rubrospinal. Moreover, the differences between the early and late components of EFP could involve interactions produced by loops between different areas, some of them projecting to the spinal cord, like cortico-rubrospinal and cortico-reticulospinal (Mediratta and Nicoll 1983; Canedo 1997; Alstermark et al. 2004; Suter and Shepherd 2015). Nevertheless, we cannot exclude that the EFP late component is generated by segmental interactions produced by intraspinal collateral branches from CS axons, which it is known are extending widely in the rostrocaudal axis and have very slow conduction velocities (Shinoda et al. 1986). In any case, timing differences in the CS control over different spinal gray matter regions could be important during voluntary movement. In this way, CS and other descending systems inhibit "sensory noise", resulting in an increase in the motoneuron signal-to-noise ratio, and hence augmenting the efficacy of motor commands (Seki et al. 2003). Thus, timing differences between dorsal vs. ventral descending commands may be important during motor execution.

Spinal neurons driven by CST

Our results suggest that the cortex has diverse outputs via the CST, modulating in a segregated manner different classes of spinal cord neuronal circuits which, together, participate in sensorimotor integration. Spinal motor neurons are directly contacted by specialized subdivision of the primates CS system, phylogenetically and ontogenetically new and originating in a particular zone of the M1 named New M1 (Griffin et al. 2015). This subsystem is particularly important for high precision and manipulatory skills involving independent finger movements. However, an indirect connection of corticospinal cells to motoneurons, through pre-motor interneurons, has been also observed both in primates (Lemon 2008) and in the mouse (Alstermark et al. 2004). In addition, the CST directly

modulates segmental interneurons involved in sensory feedback, such that the interneurons responsible for PAD are directly activated by cortex stimulation (Carpenter et al. 1963). Moreover, Clarke's column neurons (dsC), which form the dorsal spinocerebellar tract and receive proprio-ceptive-sensory inputs, are directly activated by the CST and indirectly inhibited by glycinergic and GABAergic inputs from interneurons activated by CS fibers. Thus, the CST exerts presynaptic inhibitory control over a complex interneuronal system mediating the transmission from the synaptic terminals of primary afferent fibers to spinocere-bellar neurons (Hantman and Jessell 2010). Furthermore, the segmental interneurons expressing the nuclear orphan receptor (RORα) also integrate sensory inputs from cutaneous, low-threshold mechanoreceptors, and descending signals from the cortex; this suggests the CST participates in modulating sensory information for the proper execution of voluntary movements (Bourane et al. 2015). Thus, our results raise the possibility that the cortex segregates several commands through different subpopulations of CS neurons, which may drive distinct populations of segmental inhibitory or excitatory interneurons like RORα (Bourane et al. 2015) and dSC pre-motor interneurons (Hantman and Jessell 2010), PAD-mediating interneurons (Rudomin and Schmidt 1999), or even other unexplored types.

Functional implications

The distribution profiles for the CS neurons shown here reveal that in M1, the cells projecting to the cervical dorsal horn tend to occupy the superficial portion of layer 5b, while the cells projecting to the cervical intermediate zone are located deeper within this layer (Fig. 7). Laminar differences in other layer 5b pyramidal neurons projecting subcortically have been observed. For example, the location of corticotectal cells is more superficial than that of corticotrigeminal neurons (Killackey et al. 1989). In fact, layer 5b pyramidal neurons projecting subcortically are an extremely diverse and heterogeneous population. In addition to the spinal cord, they project to several other structures like the posteromedial thalamic nucleus, superior colliculus, pontine nucleus, red nucleus, and striatum (Killackey et al. 1989; Jones and Wise 1977; Akintunde and Buxton 1992; Hattox and Nelson 2007; Groh et al. 2010). Moreover, despite the fact that in the sensorimotor cortex, all layer 5 neurons projecting to different targets are intermingled, they form segregated classes of neurons projecting mainly individually to the subcortical structures (Akintunde and Buxton 1992) and have electrophysiological (Hattox and Nelson 2007) and morphological (Killackey et al. 1989) characteristics that distinguish each class. All these targets are associated with different aspects of sensorimotor control, suggesting that these differential

projections could have functional relevance. In fact, the idea of segregated classes of different projection neurons has also been proposed by Shepherd (2013) in the context of corticostriatal connections.

The segregation of CS cells projecting to the dorsal vs. ventral aspects of the rat spinal cord shown here is analogous to what has been reported in primates, in which CST projections from M1 conspicuously avoid the dorsal horn (Coulter and Jones 1977). It is self-evident that some characteristic features, such as the skilled fore-limb control associated with bipedalism, are the product of specializations of the CS system, like corticomotoneuronal connections from the primary motor cortex. In contrast, other sensorimotor patterns have proven to be extremely successful, shaped by natural selection over extended periods of time. For example, the CS projections to the dorsal horn, exerting a control on sensory inputs from somatosensory cortices, are found in all mammals (Lemon and Griffiths 2005). Within this phylogenetic point of view, the fact that different populations of CS neurons project in a segregated manner in rats suggests that also in other species, the CST is composed of subsystems controlling different spinal cord circuits that modulate motor outputs and sensory inputs in a coordinated manner. This implies a functional and hierarchical organization among output neurons of CS layer 5 involved in the cortical circuits implicated in different aspects of motor control, and ultimately, in behavior.

References

Abdelmoumene M, Besson JM, Aleonard P (1970) Cortical areas exerting presynaptic inhibitory action on the spinal cord in cat and monkey. Brain Res 20:327–329. doi:10.1016/0006-8993(70)90301-X

Akintunde A, Buxton DF (1992) Differential sites of origin and collateralization of corticospinal neurons in the rat: a multiple fluorescent retrograde tracer study. Brain Res 575:86–92. doi:10.1016/0006-8993(92)90427-B

Alstermark B, Pettersson LG (2014) Skilled reaching and grasping in the rat: lacking effect of corticospinal lesion. Front Neurol 5:103. doi:10.3389/fneur.2014.00103

Alstermark B, Ogawa J, Isa T (2004) Lack of monosynaptic corticomotoneuronal EPSPs in rats: disynaptic EPSPs mediated via reticulospinal neurons and polysynaptic EPSPs via segmental interneurons. J Neurophysiol 91:1832–1839. doi:10.1152/jn.00820.2003

Andersen P, Eccles JC, Sears TA (1964) Cortically evoked depolarization of primary afferent fibers in the spinal cord. J Neurophysiol 27:63–77

Armand J (1982) The origin, course and terminations of corticospinal fibers in various mammals. Prog Brain Res 57:329–360. doi:10.1016/S0079-6123(08)64136-9

Babalian A, Liang F, Rouiller EM (1993) Cortical influences on cervical motoneurons in the rat: recordings of synaptic responses from motoneurons and compound action potential from corticospinal axons. Neurosci Res 16:301–310. doi:10.1016/0168-0102(93)90041-N

Baker MR, Javid M, Edgley SA (2001) Activation of cerebellar climbing fibres to rat cerebellar posterior lobe from motor cortical output pathways. J Physiol 536:825–839. doi:10.1111/j.1469-7793.2001.00825.x

Benaglia T, Chauveau D, Hunter DR, Young DS (2009) Mixtools: an R package for analyzing finite mixture models. J Stat Softw 32:1–29

Bourane S, Grossmann KS, Britz O, Dalet A, Del Barrio MG, Stam FJ, Garcia-Campmany L, Koch S, Goulding M (2015) Identification of a spinal circuit for light touch and fine motor control. Cell 160:503–515. doi:10.1016/j.cell.2015.01.011

Canedo A (1997) Primary motor cortex influences on the descending and ascending systems. Prog Neurobiol 51:287–335. doi:10.1016/S0301-0082(96)00058-5

Carpenter D, Lundberg A, Norrsell U (1963) Primary afferent depolarization evoked from the sensorimotor cortex. Acta Physiol Scand 59:126–142. doi:10.1111/j.1748-1716.1963.tb02729.x

Casale EJ, Light AR, Rustioni A (1988) Direct projection of the corticospinal tract to the superficial laminae of the spinal cord in the rat. J Comp Neurol 278:275–286. doi:10.1002/cne.902780210

Condés-Lara M, Martínez-Lorenzana G, Rojas-Piloni G, Rodríguez-Jiménez J (2007) Branched oxytocinergic innervations from the paraventricular hypothalamic nuclei to superficial layers in the spinal cord. Brain Res 1160:20–29. doi:10.1016/j.brainres.2007.05.031

Conte WL, Kamishina H, Reep RL (2009) The efficacy of the fluorescent conjugates of cholera toxin subunit B for multiple retrograde tract tracing in the central nervous system. Brain Struct Funct 213:367–373. doi:10.1007/s00429-009-0212-x

Coulter JD, Jones EG (1977) Differential distribution of corticospinal projections from individual cytoarchitectonic fields in the monkey. Brain Res 129:335–340. doi:10.1016/0006-8993(77)90012-9

Dunkerley GB, Duncan D (1969) A light and electron microscopic study of the normal and the degenerating corticospinal tract in the rat. J Comp Neurol 137:155–183. doi:10.1002/cne.901370204

Edgley SA, Jankowska E, Hammar I (2004) Ipsilateral actions of feline corticospinal tract neurons on limb motoneurons. J Neurosci 24:7804–7813. doi:10.1523/JNEUROSCI.1941-04.2004

Eguibar JR, Quevedo J, Jimenez I, Rudomin P (1994) Selective cortical control of information flow through different intraspinal collaterals of the same muscle afferent fiber. Brain Res 643:328–333. doi:10.1016/0006-8993(94)90042-6

Fink AJ, Croce KR, Huang ZJ, Abbott LF, Jessell TM, Azim E (2014) Presynaptic inhibition of spinal sensory feedback ensures smooth movement. Nature 509:43–48. doi:10.1038/nature13276

Galea MP, Darian-Smith I (1994) Multiple corticospinal neuron populations in the macaque monkey are specified by their unique cortical origins, spinal terminations, and connections. Cereb Cortex 4:166–194. doi:10.1093/cercor/4.2.166

Griffin DM, Hoffman DS, Strick PL (2015) Corticomotoneuronal cells are "functionally tuned". Science 350:667–670. doi:10.1126/science.aaa8035

Groh A, Meyer HS, Schmidt EF, Heintz N, Sakmann B, Krieger P (2010) Cell-type specific properties of pyramidal neurons in neocortex underlying a layout that is modifiable depending on the cortical area. Cereb Cortex 20:826–836. doi:10.1093/cercor/bhp152

Hantman AW, Jessell TM (2010) Clarke's column neurons as the focus of a corticospinal corollary circuit. Nat Neurosci 13:1233–1239. doi:10.1038/nn.2637

Hattox AM, Nelson SB (2007) Layer V neurons in mouse cortex projecting to different targets have distinct physiological properties. J Neurophysiol 98:3330–3340. doi:10.1152/jn.00397.2007

Hultborn H, Meunier S, Morin C, Pierrot-Deseilligny E (1987a) Assessing changes in presynaptic inhibition of I a fibres: a study in man and the cat. J Physiol 389:729–756. doi:10.1113/jphysiol.1987.sp016680

Hultborn H, Meunier S, Pierrot-Deseilligny E, Shindo M (1987b) Changes in presynaptic inhibition of Ia fibres at the onset of voluntary contraction in man. J Physiol 389:757–772. doi:10.1113/jphysiol.1987.sp016681

Jankowska E, Padel Y, Tanaka R (1976) Disynaptic inhibition of spinal motoneurones from the motor cortex in the monkey. J Physiol 258:467–487. doi:10.1113/jphysiol.1976.sp011431

Jones EG, Wise SP (1977) Size, laminar and columnar distribution of efferent cells in the sensory-motor cortex of monkeys. J Comp Neurol 175:391–438. doi:10.1002/cne.901750403

Joosten EA, Gribnau AA (1988) Unmyelinated corticospinal axons in adult rat pyramidal tract. An electron microscopic tracer study. Brain Res 459:173–177. doi:10.1016/0006-8993(88)90300-9

Kamiyama T, Kameda H, Murabe N, Fukuda S, Yoshioka N, Mizukami H, Ozawa K, Sakurai M (2015) Corticospinal tract development and spinal cord innervation differ between cervical and lumbar targets. J Neurosci 35:1181–1191. doi:10.1523/JNEUROSCI.2842-13.2015

Killackey HP, Koralek KA, Chiaia NL, Rhodes RW (1989) Laminar and areal differences in the origin of the subcortical projection neurons of the rat somatosensory cortex. J Comp Neurol 282:428–445. doi:10.1002/cne.902820309

Lawrence DG, Kuypers HG (1968) The functional organization of the motor system in the monkey. I. The effects of bilateral pyramidal lesions. Brain 91:1–14. doi:10.1093/brain/91.1.1

Leenen LP, Meek J, Posthuma PR, Nieuwenhuys R (1985) A detailed morphometrical analysis of the pyramidal tract of the rat. Brain Res 359:65–80. doi:10.1016/0006-8993(85)91413-1

Lemon RN (2008) Descending pathways in motor control. Ann Rev Neurosci 31:195–218. doi:10.1146/annurev.neuro.31.060407.125547

Lemon RN, Griffiths J (2005) Comparing the function of the corticospinal system in different species: organizational differences for motor specialization? Muscle Nerve 32:261–279. doi:10.1002/mus.20333

Lomeli J, Quevedo J, Linares P, Rudomin P (1998) Local control of information flow in segmental and ascending collaterals of single afferents. Nature 395:600–604. doi:10.1038/26975

Maeda H, Fukuda S, Kameda H, Murabe N, Isoo N, Mizukami H, Ozawa K, Sakurai M (2016) Corticospinal axons make direct synaptic connections with spinal motoneurons innervating forearm muscles early during postnatal development in the rat. J Physiol 594:189–205. doi:10.1113/JP270885

Maier MA, Perlmutter SI, Fetz EE (1998) Response patterns and force relations of monkey spinal interneurons during active wrist movement. J Neurophysiol 80:2495–2513

Martinez-Lorenzana G, Machín R, Avendaño C (2001) Definite segregation of cortical neurons projecting to the dorsal column nuclei in the rat. Neuroreport 12:413–416

Mediratta NK, Nicoll JA (1983) Conduction velocities of corticospinal axons in the rat studied by recording cortical antidromic responses. J Physiol 336:545–561. doi:10.1113/jphysiol.1983.sp014597

Miller MW (1987) The origin of corticospinal projection neurons in rat. Exp Brain Res 67:339–351. doi:10.1007/BF00248554

Moreno-Lopez Y, Perez-Sanchez J, Martinez-Lorenzana G, Condes-Lara M, Rojas-Piloni G (2013) Cortical presynaptic control of dorsal horn C-afferents in the rat. PLoS One 8:e69063. doi:10.1371/journal.pone.0069063

Nakajima K, Maier MA, Kirkwood PA, Lemon RN (2000) Striking differences in transmission of corticospinal excitation to upper limb motoneurons in two primate species. J Neurophysiol 84:698–709

Nelson RJ (1996) Interactions between motor commands and somatic perception in sensorimotor cortex. Curr Opin Neurobiol 6:801–810. doi:10.1016/S0959-4388(96)80031-6

Papp EA, Leergaard TB, Calabrese E, Johnson GA, Bjaalie JG (2014) Waxholm space atlas of the Sprague Dawley rat brain. Neuroimage 97:374–386. doi:10.1016/j.neuroimage.2014.04.001

Paxinos G, Watson C (1998) The rat brain in stereotaxic coordinates. Academic Press, London

Porter R, Lemon R (1993) Corticospinal function and voluntary movement. Oxford University Press, Oxford

Rathelot JA, Strick PL (2009) Subdivisions of primary motor cortex based on cortico-motoneuronal cells. PNAS 106:918–923. doi:10.1073/pnas.0808362106

Rojas-Piloni G, Martinez-Lorenzana G, Condes-Lara M, Rodriguez-Jimenez J (2010) Direct sensorimotor corticospinal modulation of dorsal horn neuronal C-fiber responses in the rat. Brain Res 1351:104–114. doi:10.1016/j.brainres.2010.06.010

Rudomin P, Schmidt RF (1999) Presynaptic inhibition in the vertebrate spinal cord revisited. Exp Brain Res 129:1–37. doi:10.1007/s002210050933

Rudomin P, Solodkin M, Jimenez I (1986) PAD and PAH response patterns of group Ia- and Ib-fibers to cutaneous and descending inputs in the cat spinal cord. J Neurophysiol 56:987–1006

Schieber MH (2007) Chapter 2 Comparative anatomy and physiology of the corticospinal system. Hand Clin Neurol 82:15–37

Seki K, Perlmutter SI, Fetz EE (2003) Sensory input to primate spinal cord is presynaptically inhibited during voluntary movement. Nat Neurosci 6:1309–1316. doi:10.1038/nn1154

Sengul G (2013) Atlas of the spinal cord of the rat, mouse, marmoset, rhesus, and human, 1st edn. Elsevier Academic Press, Boston

Shepherd GM (2013) Corticostriatal connectivity and its role in disease. Nat Rev Neurosci 14:278–291. doi:10.1038/nrn3469

Shinoda Y, Yamaguchi T, Futami T (1986) Multiple axon collaterals of single corticospinal axons in the cat spinal cord. J Neurophysiol 55:425–448

Stewart M, Quirk GJ, Amassian VE (1990) Corticospinal responses to electrical stimulation of motor cortex in the rat. Brain Res 508:341–344. doi:10.1016/0006-8993(90)90421-7

Sunshine MD, Cho FS, Lockwood DR, Fechko AS, Kasten MR, Moritz CT (2013) Cervical intraspinal microstimulation evokes robust forelimb movements before and after injury. J Neural Eng 10(3):036001. doi:10.1088/1741-2560/10/3/036001

Suter BA, Shepherd GM (2015) Reciprocal interareal connections to corticospinal neurons in mouse M1 and S2. J Neurosci 35:2959–2974. doi:10.1523/JNEUROSCI.4287-14.2015

Tosolini and Morris (2012) Spatial characterization of the motor neuron columns supplying the rat forelimb. Neuroscience 200:19–30. doi:10.1016/j.neuroscience.2011.10.054

Towe AL, Harding GW (1970) Extracellular microelectrode sampling bias. Exp Neurol 29:366–381. doi:10.1016/0014-4886(70)90065-8

Ullan J, Artieda J (1981) Somatotopy of the corticospinal neurons in the rat. Neurosci Lett 21:13–18. doi:10.1016/0304-3940(81)90049-5

Welniarz Q, Dusart I, Roze E (2016) The corticospinal tract: evolution, development, and human disorders. Dev Neurobiol. doi:10.1002/dneu.22455